# Multiwavelength excitation Raman scattering study of polycrystalline kesterite $Cu_2ZnSnS_4$ thin films

M. Dimitrievska,[1] A. Fairbrother,[1] X. Fontané,[1] T. Jawhari,[2] V. Izquierdo-Roca,[1,a)]
E. Saucedo,[1] and A. Pérez-Rodríguez[1,3]
[1]*Catalonia Institute for Energy Research (IREC), C. Jardins de les Dones de Negre 1, 08930 Sant Adrià del Besos, Barcelona, Spain*
[2]*Centres Científics i Technologies CCiTUB, Universitat de Barcelona, C. Lluis Sole i Sabarís 1, 08028 Barcelona, Spain*
[3]*IN2UB, Departament d'Electrònica, Universitat de Barcelona, C. Martí i Franquès 1, 08028 Barcelona, Spain*

(Received 8 October 2013; accepted 20 December 2013; published online 13 January 2014)

This work presents a complete analysis of all Raman active modes of $Cu_2ZnSnS_4$ measuring with six different excitation wavelengths from near infrared to ultraviolet. Simultaneous fitting of spectra allowed identification of 18 peaks from device grade layers with composition close to stoichiometry that are attributed to the 27 optical modes theoretically expected for this crystalline structure, including detection of 5 peaks not observed previously, but theoretically predicted. Resonance effects are assumed to explain the observed increase in intensity of weak modes for near infrared and ultraviolet excitations. These results are particularly relevant for experimental discrimination of Raman modes related to secondary phases. © *2014 AIP Publishing LLC*.
[http://dx.doi.org/10.1063/1.4861593]

Polycrystalline kesterite $Cu_2ZnSnS_4$ (CZTS) thin films have recently drawn much attention as being a promising candidate as an absorber layer in solar cell technologies,[1–3] and devices have already reached a conversion efficiency of 11.1% (Ref. 4) based on the related $Cu_2ZnSn(S,Se)_4$ compound. Optoelectronic properties of solar cells are strongly dependent on the structural properties, crystalline quality, and presence of secondary phases in the absorber layer.[5–8]

Raman spectroscopy is one of the most powerful tools for determining the crystalline structure and quality of semiconductor thin films, since the shape and position of Raman peaks are strongly influenced by the presence of defects in the material, either in the form of structural inhomogeneities or secondary phases.[9–12] In order to achieve better device performance in solar cells based on CZTS absorbers and to improve the usage of Raman spectroscopy as a control method for assessment of crystalline quality and identification of secondary phases in these promising emerging compound semiconductors, it is necessary to obtain better knowledge of their vibrational properties. Theoretical calculations on band structure, optical properties, and intrinsic defects have recently been reported.[13–16] First principle calculations done by Khare[17] and Gurel[18] have given theoretical predictions on the positions of all Raman active optical modes of the kesterite structure with the space group $I\bar{4}$ ($\Gamma = 3A \oplus 6B \oplus 6E$). The most detailed experimental study on this topic was done by Dumcencao,[19] where 14 of 27 Raman modes predicted for CZTS were identified. This included the first experimental report on the presence of a third A symmetry kesterite mode, which was deduced as a weak contribution from fitting of experimental spectra.

Usually, experimental studies for determining the Raman peaks of CZTS are done with the use of green excitation (514.5 or 532.0 nm), which is standard in Raman spectroscopy.[9,19,20] On the other hand, identification of secondary phases in CZTS in some cases cannot be done with the use of green excitation, but rather requires the use of different excitation wavelengths leading to near resonant excitation conditions for certain secondary phase compounds and they enable enhancement of their modes for more straightforward detection.[10] For example, ultraviolet (UV) excitation allows very sensitive detection of ZnS, which is the most expected secondary phase in Zn rich and Cu poor device grade CZTS layers.[21] Development of Raman scattering based procedures for detection of secondary phases in kesterite based compounds is of strong interest, because of the high impact of these phases on the optoelectronic properties of the solar cells. Detection of CZTS and secondary phases as ZnS by standard techniques such as x-ray diffraction is strongly compromised by the high level of overlapping of the main peaks in the diffractograms' characteristics for these phases.

While use of different excitation wavelengths allows identification of secondary phases, they can also induce changes in the intensities of the optical Raman modes of CZTS. For example, some Raman modes which could not be observed with standard excitation could appear with much higher intensity in the spectra measured under nonstandard excitations, and this might lead in some cases to misinterpretation with modes of secondary phases. Thus, it is important first to study the behavior of all Raman modes of CZTS in relation to different excitations, before applying this method for identification of secondary phases. First Raman spectra measured with different excitation wavelengths were reported in Ref. 12. Here, we perform a more detailed study of the whole spectral range where first order Raman CZTS modes are theoretically expected (from 50 $cm^{-1}$ up to

a)e-mail: vizquierdo@irec.cat. Tel.: + 34 933 562 615.

 

400 $cm^{-1}$), and we also extend the range of excitation wavelengths to the UV and near infrared (NIR) regions.

In this framework, this letter describes a complete analysis and identification of all active Raman modes for polycrystalline CZTS thin films using six different excitation wavelengths (325.0, 457.9, 514.5, 632.8, 785.0, and 830.0 nm). In principle, near resonance Raman effects are expected to be the main factors influencing changes in the Raman spectra of CZTS with the excitation wavelength. Tuning the incident laser to resonate with a strong electronic inter-band transition enables the enhancement of the Raman cross section, and vibrational modes associated with that particular transition exhibit an increase in intensity.[22]

According to theoretical calculations for electronic band structure of kesterites done by Kumar and Persson,[23] the estimated energy, for CZTS, of the $\Gamma_1$ point (band gap energy) is 1.47 eV, while the energy of the $\Gamma_2$ point is around 3.50 eV. Taking into account the values of energies for $\Gamma_1$ and $\Gamma_2$ points, the excitation wavelengths of 830.0, 785.0, and 325.0 nm, with corresponding energies of 1.49, 1.58, and 3.82 eV could be considered as good conditions for near resonance Raman scattering effects. In principle, increasing in intensity of the Raman modes because of near resonant excitation conditions is expected to take place especially for E and B symmetry modes, which are NIR active and have TO/LO splitting due to their polar character.[17,22] It is interesting to remark that these modes are only observed as very weak peaks in standard Raman scattering conditions, where the spectra are dominated by the two main A symmetry modes at 287 and 338 $cm^{-1}$, which are not NIR active.

For the present letter, CZTS thin films of photovoltaic grade with high crystalline quality were investigated. The samples were prepared by thermal treatment of metallic precursors made by DC-magnetron sputtering deposition onto soda-lime glass/Mo substrates. Prototype solar cell devices made with these films give promising efficiency values up to 5.5%. More details about precursor deposition, thermal processing, device fabrication, and characterization can be found elsewhere.[21] External quantum efficiency (EQE) measurements performed on these cells give a band gap estimation of 1.46 eV, close to the value calculated for the $\Gamma_1$ point energy. Compositional ratios of the as-annealed films were approximately $Cu/(Zn+Sn)=0.82$ and $Zn/Sn=1.24$. These non-stoichiometric composition conditions are typically required to achieve devices with reasonable efficiency.[8] These conditions inhibit formation of detrimental Cu-Sn-S ternary phases, although they might favour formation of the ZnS secondary phase. To remove this secondary phase from the surface of the films, a selective chemical etching for ZnS has been performed with a HCl solution.[24] After etching with this solution, the composition ratios change to values closer to a stoichiometric composition ($Cu/(Zn+Sn)=0.96$ and $Zn/Sn=1.09$). The spectra presented in this letter correspond to the as-etched sample. As previously reported,[21] Zn-excess remaining in the etched film tends to be mainly concentrated at the back contact region, and we can consider that the surface is free of ZnS. This is corroborated by Raman scattering measurements performed with UV excitation, as will be discussed later.

Raman scattering measurements were performed in back scattering configuration with a LabRam HR800-UV and T64000 Horiba-Jobin Yvon spectrometers. For the HR800-UV system, diode-pumped solid state lasers with wavelengths of 785.0 and 830.0 nm, and gas HeCd and HeNe lasers with wavelengths of 325.0 and 632.8 nm, respectively, were used for excitation. In this system, excitation and light collection were made through an Olympus metallographic microscope, with a laser spot size on the order of 1–2 $\mu$m (depending on the excitation wavelength). To avoid effects in the spectra related to potential microscopic inhomogeneities, the spot was rastered over an area of $30\times30\ \mu m^2$. Furthermore, the T64000 system works coupled with an ion-Ar+ laser, and measurements were made with 514.5 nm and 457.9 nm excitation lines, with a 100 $\mu$m spot size on the sample. In all cases, and to avoid the presence of thermal effects in the spectra, the power excitation density was around 50 $W/cm^2$. The first-order Raman spectrum of monocrystalline Si was measured as a reference before and after acquisition of each Raman spectrum, and the spectra were corrected with respect to the Si line at 520 $cm^{-1}$.

Figure 1 presents the experimental Raman spectra of measured CZTS sample under different excitation wavelengths. Simultaneous fittings of spectra with Lorentzian curves have allowed identification of 18 peaks attributed to the 27 optical modes, which are expected according to the zone center phonon representation. The position of each Raman peak, the excitation condition under which it is most intense, and symmetry assignment is presented in Table I.

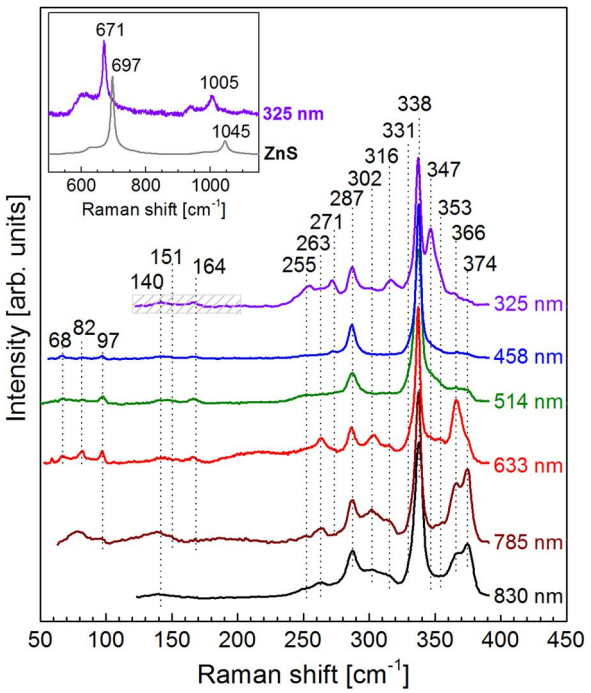


FIG. 1. Raman spectra of polycrystalline $Cu_2ZnSnS_4$ thin film measured with different excitation wavelengths with indication of the characteristic peaks. Dashed region presented in the spectrum measured with 325 nm wavelength corresponds to the region of strong attenuation originating from the Raman edge filter. Presence of Raman peaks in this region suggests strong enhancement of the modes expected in this spectral interval. Spectra are arbitrarily vertically shifted for more clarity. Inset shows the spectra measured in the 500–1150 $cm^{-1}$ region with 325 nm excitation wavelength from the $Cu_2ZnSnS_4$ thin film and a reference ZnS layer.

In addition, Table I also contains theoretical calculations[17,18] and previously reported experimental data.[9,19,20] The symmetry assignment of Raman modes was done by comparing the experimentally obtained frequencies with the reported references as well as with polarization measurements done for these samples. Inset in Figure 1 shows the Raman spectra measured with 325 nm excitation wavelength in the CZTS sample and in a reference ZnS sample, in the 500–1150 $cm^{-1}$ spectral range. The spectrum from the reference ZnS sample shows the peaks at 697 and 1045 $cm^{-1}$ corresponding to the second and third order peaks of the main ZnS Raman mode. Presence of these peaks is due to the existence of a quasi-resonant excitation of the main ZnS Raman mode at this excitation wavelength.[10] Absence of these peaks characteristic of the ZnS phase from the spectrum measured in the CZTS layer corroborates the absence in the surface region of this layer of a ZnS secondary phase. Additionally, the CZTS second (region between 550 and 750 $cm^{-1}$) and third (region between 900 and 1050 $cm^{-1}$) spectral regions are also observed in the spectrum, including the second and third order CZTS peaks at 670.9 and 1004.7 $cm^{-1}$, respectively.

Figure 2 shows a plot of the spectra measured with 325.0, 514.5 nm, 632.8, and 785.0 nm excitation wavelengths normalized to the intensity of the main peak at 337.5 $cm^{-1}$. Spectra measured with 325.0 nm are characterized by a strong increase in the relative intensity of the Raman peaks at 255.1, 271.1, 315.9, and 347.3 $cm^{-1}$ in relation to those from the spectra measured with standard 514.5 nm excitation. Similarly, relative intensity of peaks at 139.8, 150.7, 262.7, 366.6, and 374.4 $cm^{-1}$ increases for 785.0 nm excitation. These results agree with the expected enhancement in the intensity of CZTS polar vibrational modes taking into account the possible existence of a near resonant behavior. In addition, spectra measured with 632.8 nm also show an increase in the relative intensity of the peaks that are located at 81.5, 96.9, 262.7, and 366.6 $cm^{-1}$. This could be due to the existence also in this case of a near resonant excitation behavior, even if the energy is not so close to those of the $\Gamma_1$ and $\Gamma_2$ CZTS points.

TABLE I. Frequency (in $cm^{-1}$) of peaks from simultaneous fitting of Raman spectra measured with different excitation wavelengths, excitation condition under which the peak is best resolved, and proposed mode symmetry assignment. These are compared with theoretical predictions[17,18] and other reported experimental data.[9,19,20]

| This work | | Theoretical predictions | | | Experimental reported | | |
|---|---|---|---|---|---|---|---|
| $\lambda$[a] [nm] | RS[b] [$cm^{-1}$] | Sym[c] | RS[d] [$cm^{-1}$] | RS[e] [$cm^{-1}$] | RS[f] [$cm^{-1}$] | RS[g] [$cm^{-1}$] | IR[h] [$cm^{-1}$] |
| 633 | 67.8 | E | 79.2 E(TO/LO) | 82.2 E(TO/LO) | 66 | | 68 (IR) |
| 633 | 81.5 | B | 92.3 B(TO)/93.1 B(LO) | 87.8 B(TO)/88.2 B(LO) | 83 | | 86 (IR) |
| 633 | 96.9 | E/B | 101.4 E(TO/LO)/104.2 B (TO)/104.3 B(LO) | 99.3 B(TO/LO)/102.9 E(TO)/ 103.0 E(LO) | 97 | | |
| 785 | 139.8 | E | 166.1 E(TO) | 150.0 E(TO) | 143 | 143 E(TO) | 143 (IR) |
| 785 | 150.7 | E | 166.2 E(LO) | 150.5 E(LO) | | 145 E(LO) | |
| 325 | 164.1 | B | 179.6 B(TO)/179.9 B(LO) | 168.2 B(TO)/169.5 B(LO) | 166 | 160 B(TO) 162 B(LO) | 168 (IR) |
| 325 | 255.1 | B/E | 269.1 B(TO)/278.2 E(TO) | 237.9 B(TO)/247.8 E(TO) | 252 | 245 B(TO) 250 B(LO) 255 E(LO) | 255 (IR) |
| 633 | 262.7 | B | 285.1 B(LO) | 253.7 B(LO) | | | |
| 325 | 271.1 | E | 289.8 E(LO) | 254.8 E(LO) | 272 | | 293(IR) |
| 830 | 287.1 | A | 302.1 A | 281.7 A | 287 | 285 A | |
| 785 | 302.1 | A | 309.0 A | 270.0 A | | 306 A | |
| 325 | 315.9 | E | 309.7 E(TO)/ 314.1 E(LO) | 278.0 E(TO)/ 290.5 E(LO) | | | 316 (IR) |
| 325 | 331.9 | B | 332.7 B(TO)/ 336.1 B(LO) | 307.6 B(TO)/ 311.4 B(LO) | | | |
| 514 | 337.5 | A | 335.2 A | 338.5 A | 337 | 334 A | |
| 325 | 347.3 | E | 341.4 E(TO) | 351.1 E(TO) | 347 | 341 E(TO) 346 E(LO) | |
| 514 | 353.0 | B | 354.8 B(TO) | 357.0 B(TO) | 353 | 352 B(TO) 353 B(LO) | 351 (IR) |
| 633 | 366.6 | E | 353.3 E(LO) | 365.3 E(LO) | | | |
| 785 | 374.4 | B | 366.4 B(LO) | 373.6 B(LO) | | | |

[a]$\lambda$ is the excitation wavelength.
[b]RS is the Raman shift from this work.
[c]Sym is the symmetry proposed in this work.
[d]RS is the Raman shift reported in Ref. 17.
[e]RS is the Raman shift reported in Ref. 18.
[f]RS is the Raman shift reported in Ref. 9.
[g]RS is the Raman shift reported in Ref. 19.
[h]IR are the infrared absorption frequencies reported in Ref. 20.

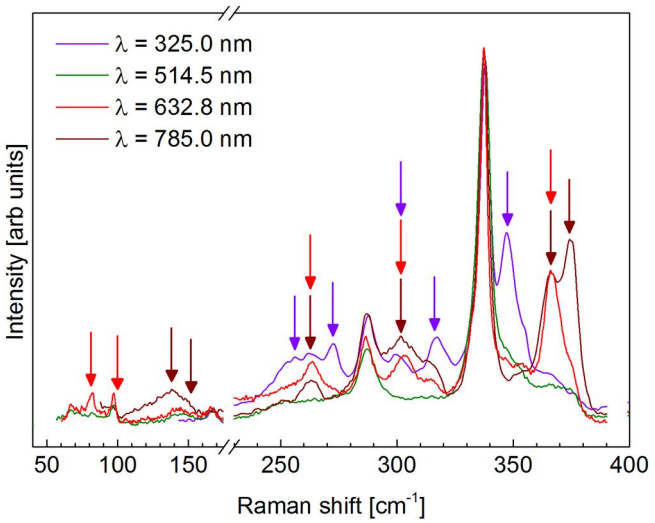


FIG. 2. Comparison between Raman spectra measured with standard green excitation (514.5 nm), and measurements made with 325.0, 632.8, and 785.0 nm excitation. The colored arrows indicate the excitation wavelength for which each particular band has the greatest increase in intensity.

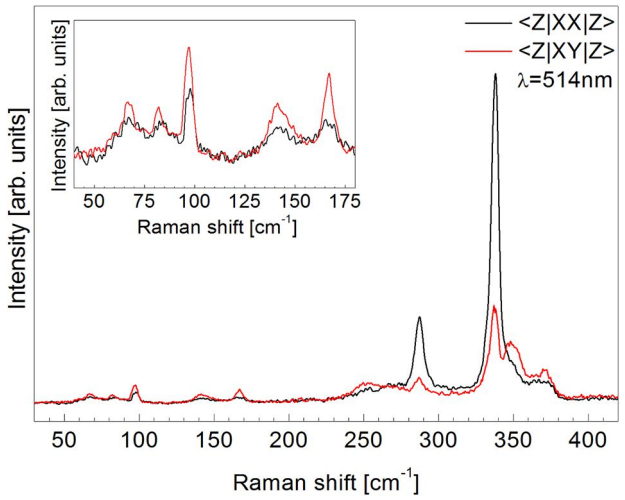


FIG. 3. Raman polarization measurements of $Cu_2ZnSnS_4$ done in parallel and perpendicular polarization configurations (excitation wavelength 514.5 nm).

In addition, these excitation conditions also allow observation of a well resolved peak at 302.1 $cm^{-1}$, that according to simulation data, has been identified as the third A symmetry mode from the CZTS kesterite phase.[19] Even though Dumcencao[19] already reported the existence of this mode, it is interesting to remark that in their work the presence of this mode was deduced from deconvolution of the experimental spectra, and the peak was not experimentally resolved in their spectra, as is done here.

In the case of the peak at 347.3 $cm^{-1}$ observed with UV excitation conditions, an increase in the intensity of a peak in this spectral region has previously been attributed to the presence of a ZnS secondary phase, because of the existence of a quasi-resonant excitation of ZnS in these measuring conditions.[10] However, experimentally, presence of this phase is also accompanied by the detection of the second order ZnS peak at 697 $cm^{-1}$ spectral region. Absence of this second order peak in the spectra from the samples analyzed in this work (as shown in the inset in Figure 1) supports its identification as a mode characteristic of the CZTS compound, unrelated to the presence of a ZnS secondary phase.

On the other hand, fitting of the spectra gives also a contribution at 331.9 $cm^{-1}$, which has been identified with a B symmetry mode, in agreement with the theoretical data. However, this is also close to a peak at 331 $cm^{-1}$, which has been related to the presence of local inhomogeneities with a high degree of disorder in the cation sublattice of CZTS, as reported by Fontané *et al.*[9] for bulk powder samples. More recent studies from single crystal bulk samples with different compositions[25] have identified this peak with the main $A_1$ symmetry mode from the disordered kesterite phase, which is characterized by a random distribution of Cu and Zn cations in the Cu-Zn planes. This leads to a change in the group symmetry to the stannite-like $I\bar{4}m2$. In contrast with the behavior shown in Figure 2, presence of this disordered kesterite phase in the bulk and single crystal samples reported in Refs. 9 and 25 is characterized by an intense and broad peak in this spectral region in the spectrum measured with 514.5 nm excitation. This suggests that conditions related to the growth of bulk samples, which typically involve higher temperature thermal treatments than those used for the synthesis of the device grade polycrystalline thin films, favor formation of this disordered phase when working under non-stoichiometric conditions.

Confirmation of proposed symmetry types could be done with comparison to polarized Raman spectra measurements for CZTS, as seen in Figure 3. According to Raman tensors for the space group $I\bar{4}$ (Ref. 17) and calculations of depolarization ratio for the polycrystalline films with random orientation, in the case of change in polarization conditions from parallel $\langle Z|XX|Z\rangle$ to perpendicular $\langle Z|XY|Z\rangle$ configurations, the intensity of all A modes would always decrease, while the intensity of all E modes would always increase. In case of B modes, their intensity could increase or decrease depending on their type. From the results shown in Figure 3, it can be seen that intensities of all peaks increase with the change in polarization, except for peaks in spectral region from 270 to 340 $cm^{-1}$, which decrease in intensity. This indicates that all A modes must be positioned in this region, which is in accord with the multiwavelength excitation results.

In conclusion, this work demonstrates the utility of multiwavelength excitation for the deeper vibrational characterization of device grade polycrystalline CZTS. In addition to allowing easier identification of 11 peaks previously observed with standard green excitation,[9,19,20] the analysis performed here also allows experimental observation and symmetry assignment of 5 Raman peaks characteristic for CZTS with positions at 262.7, 315.9, 331.9, 366.6, and 374.4 $cm^{-1}$, which were not previously experimentally reported, but are theoretically predicted. The symmetry assignment of these peaks is performed according to polarization measurements and the theoretical calculations done by Gurel *et al.*[17] and Khare *et al.*[18] This knowledge is especially relevant for the further development of multiwavelength Raman scattering based methodologies for detection of secondary phases, which is still required for further optimization of these technologies.

The research leading to these results has received funding from the People Program (Marie Curie Actions) of the European Union's Seventh Framework Program FP7/2007-2013/ under REA Grant Agreement No. 316488 (KESTCELLS), and from project KEST-PV (Ref. ENE2010-121541-C03-1) from the Spanish "Ministerio de Economia y Competitividad." Authors from IREC and IN$^2$UB belong to the M-2E (Electronic Materials for Energy) Consolidated Research Group and the XaRMAE Network of Excellence on Materials for Energy of the "Generalitat de Catalunya." E.S. thanks the Government of Spain for the "Ramon y Cajal" fellowship (RYC-2011-09212) and V.I. for the "Juan de la Cierva" fellowship (JCI-2011-10782) and A.F. thanks the Spanish Government for the FPU Fellowship (FPU12/05508).

[1]C. A. Wolden, J. Kurtin, J. B. Baxter, I. Repins, S. E. Shaheen, J. T. Torvik, A. A. Rockett, V. M. Fthenakis, and E. S. Aydil, J. Vac. Sci. Technol., A **29**, 030801 (2011).
[2]H. Katagiri, Thin Solid Films **480–481**, 426 (2005).
[3]T. Kato, H. Hiroi, N. Sakai, S. Muraoka, and H. Sugimoto, in *27th European PV Solar Energy Conference and Exhibition* (2013), p. 2236.
[4]T. Todorov, J. Tang, S. Bag, O. Gunawan, Y. Zhu, and D. Mitzi, Adv. Energy Mater. **3**, 34 (2013).
[5]S. Schorr, Sol. Energy Mater. Sol. Cells **95**, 1482–1488 (2011).
[6]A. Redinger, D. M. Berg, P. J. Dale, and S. Siebentritt, J. Am. Chem. Soc. **133**, 3320 (2011).
[7]S. Chen, X. G. Gong, A. Walsh, and S.-H. Wei, Appl. Phys. Lett. **96**, 021902 (2010).
[8]D. B. Mitzi, O. Gunawan, T. K. Todorov, K. Wang, and S. Guha, Sol. Energy Mater. Sol. Cells **95**, 1421 (2011).
[9]X. Fontane, V. Izquerdo-Roca, E. Saucedo, S. Schorr, V. O. Yukhymchuk, M. Ya. Valakh, A. Perez-Rodrigez, and J. R. Morante, J. Alloys Compd. **539**, 190 (2012).
[10]X. Fontané, L. Calvo-Barrio, V. Izquierdo-Roca, E. Saucedo, A. Pérez-Rodriguez, J. R. Morante, D. M. Berg, P. J. Dale, and S. Siebentritt, Appl. Phys. Lett. **98**, 181905 (2011).
[11]A.-J. Cheng, M. Manno, A. Khare, C. Leighton, S. A. Campbell, and E. S. Aydil, J. Vac. Sci. Technol., A **29**, 051203 (2011).
[12]P. A. Fernandes, P. M. P. Salome, and A. F. da Cunha, J. Alloys Compd. **509**, 7600–7606 (2011).
[13]S. Chen, X. G. Gong, A. Wals, and S. H. Wei, Phys. Rev. B **79**, 165211 (2009).
[14]C. Persson, J. Appl. Phys. **107**, 053710 (2010).
[15]A. Nagoya, R. Asahi, R. Wahl, and G. Kresse, Phys. Rev. B **81**, 113202 (2010).
[16]S. Chen, J. H. Yang, X. G. Gong, A. Walsh, and S. H. Wei, Phys. Rev. B **81**, 245204 (2010).
[17]T. Gurel, C. Sevik, and T. Cagin, Phys. Rev. B **84**, 205201 (2011).
[18]A. Khare, B. Himmetoglu, M. Cococcioni, and E. S. Aydil, J. Appl. Phys. **111**, 123704 (2012).
[19]D. Dumcenco and Y.-S. Huang, Opt. Mater. **35**, 419–425 (2013).
[20]M. Himmrich and H. Haeuseler, Spectrochim. Acta A **47**, 933 (1991).
[21]A. Fairbrother, X. Fontané, V. Izquierdo-Roca, M. Espíndola-Rodríguez, S. López, M. Placidi, L. Calvo-Barrio, A. Pérez-Rodríguez, and E. Saucedo, Sol. Energy Mater. Sol. Cells **112**, 97–105 (2013).
[22]P. Y. Yu and M. Cardona, *Fundamentals of Semiconductors*, 4th ed. (Springer, Berlin, 2010), p. 401.
[23]M. Kumar and C. Persson, Int. J. Theor. Appl. Sci. **5**(1), 1 (2013).
[24]A. Fairbrother, E. Gracia-Hemme, V. Izquierdo-Roca, X. Fontane, F. A. Pulgarin-Agudelo, O. Vigil-Gala, A. Perez-Rodrigez, and E. Saucedo, J. Am. Chem. Soc. **134**, 8018 (2012).
[25]M. Y. Valakh, O. F. Kolomys, S. S. Ponoaryov, V. O. Yukhymcuk, I. S. Babichuk, V. Izquierdo-Roca, E. Saucedo, A. Perez Rodrigez, J. R. Morante, S. Schorr, and I. V. Bodnar, Phys. Status Solidi (RRL) **7**, 258 (2013).